Identification of Small-Molecule Inhibitors of Human Angiogenin and Characterization of Their Binding Interactions Guided by Computational Docking†

Jeremy L. Jenkins‡ and Robert Shapiro*,‡,§

Center for Biochemical and Biophysical Sciences and Medicine and Department of Pathology, Harvard Medical School, Boston, Massachusetts 02139

Received January 30, 2003; Revised Manuscript Received April 2, 2003

ABSTRACT: Angiogenin (ANG) is a potent inducer of angiogenesis and an RNase A homologue whose ribonucleolytic activity is essential for its biological action. Recently, we reported the identification of small non-nucleotide inhibitors of the enzymatic activity of ANG by high-throughput screening (HTS) [Kao, R. Y. T., et al. (2002) *Proc. Natl. Acad. Sci. U.S.A. 99,* 10066−10071]. Two of the inhibitors that were obtained, National Cancer Institute compound NSC-65828 [8-amino-5-(4′-hydroxybiphenyl-4-ylazo)-naphthalene-2-sulfonate] and ChemBridge compound C-181431 [4,4′-dicarboxy-3,3′-bis(naphthylamido)-diphenylmethanone], were judged to be suitable for further development, and one of these (NSC-65828) was shown to possess antitumor activity in mice. Here we have used computational docking as a guide for the identification of available NSC-65828 and C-181431 analogues that bind more tightly to ANG, and for the characterization of inhibitor binding modes. Numerous analogues were found to have greater avidity than the HTS compounds or any small nucleotide inhibitors; four were considered to be of interest as potential leads ($K_i = 5-25\ \mu M$). Two of these analogues bind more tightly to ANG than to RNase A, and are the first small molecules shown to exhibit this selectivity. The predicted binding orientations of the HTS compounds and the new lead inhibitors were evaluated by determining the effects of ANG active site mutations on inhibitory potency. The results with ANG variants R5A, H8A, N68A, and des(121−123) are highly consistent with the docking models. Affinity changes observed with Q12A and Q117G reveal aspects of active site function that are not apparent from the free ANG crystal structure or from the modeled complexes. These findings should prove to be useful in the design of more effective and specific ANG antagonists.

Angiogenin (ANG)[1] is a member of the pancreatic RNase superfamily whose sequence is 33% identical to that of RNase A (*1*). It is unique among RNases in that it is a potent inducer of angiogenesis in vivo (*2*). Its enzymatic properties are also distinctive: most notably, the ribonucleolytic activity of ANG toward standard RNase substrates is extremely weak, typically 10^5-10^6 times lower than that of RNase A (*3*−*5*). Despite this weakness, studies with variants and inhibitors have indicated that the enzymatic activity of ANG is critical for angiogenic activity (*6*−*9*). Although the precise molecular mechanism by which ANG induces the formation of new blood vessels has not been determined, evidence to date suggests that the nucleolus of endothelial cell targets is an important site of action (*10*) and that ANG functions there to promote ribosome biogenesis required for cell proliferation (*11*). This might then provide a biological "rationale" for ANG's catalytic inefficiency, since a robust general RNase would be highly destructive in such an RNA-rich locale (*12*).

ANG was first isolated from human tumor cell-conditioned medium (*2*), and clinical studies have since shown ANG expression to be increased in at least 12 different types of cancer; in some instances, a specific association between high ANG levels and cancer progression or poor prognosis has also been demonstrated (see refs *13*−*15*). Moreover, several ANG antagonists, including monoclonal antibodies, antisense oligonucleotides, the ANG-binding protein actin, and an ANG-binding peptide, have proven to be highly effective at inhibiting the establishment and/or metastatic dissemination of human tumors in athymic mice (*16*−*18*). These findings identify ANG as a potentially important target for new anticancer drugs. Clearly, small-molecule inhibitors would have major advantages over the aforementioned antagonists for pharmaceutical applications. In developing such compounds, we have focused primarily on the ribonucleolytic site of ANG because of its key role in the biological activity of this protein and the considerable success record of targeting enzymatic active sites for drug discovery in general.

ANG has a relatively low avidity for all nucleotides examined thus far (*19*, *20*), suggesting that standard ap-

† This work was supported by the National Institutes of Health (Grant CA88738 to R.S.) and the National Cancer Institute Developmental Therapeutics Program (R*A*N*D project "Optimization of small-molecule lead compounds for inhibition of angiogenin").

* To whom correspondence should be addressed: Center for Biochemical and Biophysical Sciences and Medicine, One Kendall Square, Building 600, 3rd Floor, Cambridge, MA 02139. Phone: (617) 621-6132. Fax: (617) 621-6111. E-mail: Robert_Shapiro@hms.harvard.edu.

‡ Center for Biochemical and Biophysical Sciences and Medicine.

§ Department of Pathology.

[1] Abbreviations: ANG, angiogenin; RNase A, bovine pancreatic ribonuclease A; HTS, high-throughput screening; LC−MS, liquid chromatography−mass spectrometry; des(121−123), recombinant ANG in which the C-terminal peptide of residues 121−123 has been deleted; rmsd, root-mean-square deviation.

10.1021/bi034164e CCC: $25.00
Published on Web 05/13/2003

proaches for generating enzyme inhibitors based on substrate or product analogues may be difficult in this case. Therefore, we recently explored a pathway for identifying non-nucleotide antagonists by high-throughput screening (HTS) (*9*). Two of the inhibitors that were obtained, NSC-65828 (henceforth termed compound **1**) and C-181431 (compound **2**), were considered especially suitable for further development. Compound **1** was shown to delay or prevent the establishment of PC3 and HT29 human tumor xenografts in athymic mice, whereas an analogue with no detectable effect on the ribonucleolytic activity of ANG did not impede tumor growth. The data from this study strongly support the strategy of targeting the ANG active site and suggest that compounds with increased antiribonucleolytic potency might be even more efficacious as therapeutic agents.

The availability of a high-resolution crystal structure of ANG (*21*) enables "rational" approaches for lead optimization. Ideally, this route would utilize as its starting point a crystal or NMR structure of an ANG−inhibitor complex. However, structural studies on complexes with compounds **1** and **2** have been hampered by the limited aqueous solubility of these inhibitors (K. R. Acharya, J. L. Jenkins, and R. Shapiro, unpublished observations) and unfortunate intermolecular contacts in all ANG crystals grown thus far (*22*). In previous cases where protein−ligand complex structures were unavailable, computational ligand docking has often been a powerful tool for predicting binding configurations of newly discovered leads and facilitating rational design (*23*, *24*). For ANG, comparison of the results of computational high-throughput docking with those from HTS of the same chemical library (*25*) suggests that docking may also be useful with this target.

Here we have used models of the complexes of ANG with compounds **1** and **2** generated by the AutoDock Lamarckian Genetic Algorithm (*26*) as a basis for searching chemical databases for available analogues that might have improved inhibitory activity. This led to the identification of numerous compounds that bind more tightly than the original inhibitors, four of which we judge to be of interest as potential leads. The predicted binding orientations, or "poses", of these analogues and the original compounds were then evaluated by measuring the effects of ANG active site residue replacements on inhibitory potency. The specificity of the various compounds for ANG versus RNase A was also assessed, and was interpreted with respect to docked complexes with the two proteins. Our results are largely consistent with the models, but reveal aspects of active site function that are not apparent from either the crystallographically determined structure of free ANG or the predicted complex structures. These findings should prove to be useful for the design of new ANG antagonists based on the compounds now in hand as well as future active site-directed inhibitors.

EXPERIMENTAL PROCEDURES

Materials. Human ANG and its R5A, Q117G, des(121−123), H8A, Q12A, and N68A variants were produced with a recombinant system in *Escherichia coli* as reported previously (*27*−*30*). Testing with an inhibitor that greatly prefers RNase A over ANG showed that the ANG preparation was essentially free of contamination by adventitious RNase A (*9*). The strong cytidine versus uridine selectivity of the variant preparations also indicated that these did not contain any significant RNase A (*31*). Sources of RNase A and substrates for enzymatic reactions were listed previously (*9*, *32*). The preparation of compound **1** [8-amino-5-(4′-hydroxybiphenyl-4-ylazo)naphthalene-2-sulfonate] used for kinetic determinations was the resynthesized material reported previously (*9*). The other compounds tested as inhibitors of ANG were from the National Cancer Institute (NSC series), ChemBridge Corp. (C series), or Sigma-Aldrich. The six inhibitors characterized in detail were judged to be >95% pure by thin-layer silica gel chromatography [10:10:2:1 (v/v) 2-butanol/ethanol/water/ammonium hydroxide mixture]. Additional analytical information about compound **1** was reported previously (*9*). NSC-65820 [6-hydroxy-5-(2-hydroxy-3,5-dinitrophenylazo)naphthalene-2-sulfonate] and benzopurpurin B [3,3′-dimethylbiphenyl-4,4′-bis(2-aminonaphthylazo-6-sulfonate), Sigma-Aldrich] were analyzed by liquid chromatography−mass spectrometry (LC−MS) on a Micromass Platform LCZ instrument with electrospray ionization. LC was performed on a C18 column (YMC ODS-AQ, 2.0 mm × 50 mm, particle size of 3 μm) in 0.1% formic acid with a 15 to 100% acetonitrile gradient over 5 min at a flow rate of 0.8 mL/min at 50 °C. $[M - H]^-$ was 432.9 Da versus 433.0 Da (calcd) for NSC-65820 and 679.0 Da versus 678.1 Da (calcd) for benzopurpurin B. MS data confirming the structures of compound **2** [4,4′-dicarboxy-3,3′-bis(naphthylamido)diphenylmethanone], C-473872 [3,3′-dicarboxy-4,4′-bis(4-biphenylamido)diphenylmethane], and C-467929 [3,3′-dicarboxy-4,4′-bis(3-nitrophenylamido)diphenylmethane] were provided by the supplier. For most of the compounds that were examined, concentrations were based on weight, except that spectrophotometric determinations were performed in those cases where published extinction coefficients were available (*33*).

Molecular Modeling and Docking. Molecular visualization was carried out in InsightII (Accelrys, Inc., San Diego, CA) on a Silicon Graphics IndigoII Maximum Impact workstation. Protein coordinates for docking included a 1.8 Å resolution X-ray structure of free ANG (PDB entry 1B1I), a modified version of this structure in which C-terminal residues 119−123 have been deleted, a 1.8 Å resolution structure of Q117G ANG (PDB entry 1K59), and a 2.0 Å resolution structure of free RNase A (PDB entry 1AFU). Compound structures were obtained from the NCI Developmental Therapeutics Program website (http://dtp.nci.nih.gov/), Sigma-Aldrich, and ChemBridge Corp. (www.chembridge.com). Where necessary, two-dimensional structures were converted to three-dimensional structures and energy minimized in Chem3D (CambridgeSoft). Waters were removed from protein PDB files, and hydrogens were assigned in InsightII; potentials and partial charges for proteins and compounds were assigned with the CFF91 force field, and structures were saved as Sybyl mol2 files. Rotatable bonds in the ligands were assigned with the program AutoTors in AutoDock; all N═N bonds were made unrotatable. Ligand docking was carried out with the AutoDock 3.0.5 Lamarckian Genetic Algorithm (*26*). The binding free energies calculated by this program are based on an empirical function derived by linear regression analysis of protein−ligand complexes with known binding constants; this function includes terms for changes in energy due to van der Waals, hydrogen bonding, and electrostatic forces, as well as ligand torsion and desolvation.

The AutoDock default parameters were employed for docking, except that 10 runs with 1.5×10^6 energy evaluations each were used and ligand centers were initially positioned at the grid centers. The docking energy grid (22.50 Å^3 for compounds **1** and **1a** and 26.25 Å^3 for the other compounds, which are larger) was produced with the AutoGrid program. Grids were centered at the position occupied by the phosphorus atom in the superimposed coordinates of the ANG−phosphate complex (PDB entry 1H52) and each ANG or RNase A structure. After docking had been carried out, the 10 positions were sorted into clusters with 1 Å root-mean-square deviations (rmsd), and the lowest-energy docking pose was used for analysis. The reported rmsd values are with respect to the lowest-energy pose, and were determined with the executable "RMSD" from DOCK 4.0 (*34*).

Analogue Searching and Prioritization. NCI, the Available Chemicals Directory (ACD), and ChemBridge libraries were searched for analogues as described in the Results and Discussion. ACD was accessed using Isis/Base version 2.2 (MDL Information System, Inc.). NCI and ChemBridge databases were searched directly through their websites. In those instances where analogue hit lists were prioritized for testing by high-throughput docking, the program DockVision (*35*) was used and the poses were scored in Ludi (*36*) as described previously (*25*), except that the van der Waals radii parameter in DockVision ("pvdw Radius") was softened from 4 to 6 because this was found to position test ligands NSC-65828 and C-181431 more closely to AutoDock-generated poses.

HPLC-Based Inhibition Assays. K_i values were determined from the dependence of k_{cat}/K_m values for cleavage of the octanucleotide substrate $(dA)_5rC(dA)_2$ on inhibitor concentration. Except where otherwise noted, test compounds were incubated with 5 μM ANG and 20 μM substrate [expected to be well below the K_m (*28*, *37*)] in 20 mM Hepes-NaOH and 100 mM NaCl (pH 7) (buffer A) at 37 °C for 2 h. Substrate and cleaved product were resolved by Mono Q anion-exchange chromatography, and their peak areas were used to calculate k_{cat}/K_m values (*9*, *38*). Inhibitors were screened initially at 50 or 75 μM for NSC-65828 analogues, and at 25 or 50 μM for C-181431 analogues, and inhibition constants were calculated as $[I_t(k_{cat}/K_m)_i]/[(k_{cat}/K_m)_0 - (k_{cat}/K_m)_i]$, where $(k_{cat}/K_m)_i$ and $(k_{cat}/K_m)_0$ are values measured in the presence and absence of inhibitor, respectively, and I_t is the total inhibitor concentration. For the six analogues studied in detail, at least six concentrations were used to obtain final K_i values, which were calculated by fitting the data to the equation (*39*)

$$(k_{cat}/K_m)_i = [(k_{cat}/K_m)_0/2E_t]\{[(K_i + I - E_t)^2 + 4K_iE_t]^{1/2} - (K_i + I - E_t)\}$$

in SigmaPlot 2000 (SPSS), where E_t is the total concentration of the enzyme; this treatment takes into account depletion of free inhibitor by enzyme. K_i values were also measured in 200 mM Mes-NaOH (pH 5.9) (buffer B) at 25 °C, the conditions used previously for nucleotide inhibitors. ANG has ~10-fold higher activity in this assay, and the enzyme concentration and incubation time were therefore decreased to 1 μM and 1 h, respectively. Assays used to assess the effect of salt concentration on binding to ANG were carried out at 37 °C in 20 mM Mes-NaOH (pH 5.9) containing 20, 100, and 200 mM NaCl (i.e., 26, 106, and 206 mM total Na^+, respectively) with 0.5, 2, and 5 μM ANG, respectively; incubation times were 50 min, 1 h, and 2 h, respectively. The enzymatic potencies of ANG variants differ considerably, and it was therefore necessary to tailor enzyme concentration, incubation time, and buffer for K_i determinations individually: 5 μM, 2 h, and buffer B for R5A; 5 μM, 1 h, and buffer B for H8A; 1 μM, 1 h, and buffer B for Q12A; 1 μM, 1 h, and buffer B for N68A; 2 μM, 1 h, and buffer B for des(121−123); and 0.5 μM, 50 min, and buffer A for Q117G. Reactions in buffer A and buffer B were carried out at 37 and 25 °C, respectively.

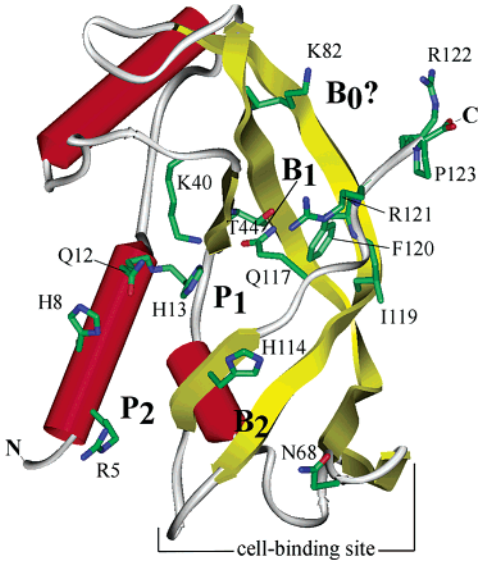

FIGURE 1: Schematic representation of the crystal structure of ANG (PDB entry 1B1I) showing secondary structural elements (cylinders for α-helices and ribbons for β-strands) and side chains of active site residues, drawn with InsightII (Accelrys). The positions of the subsites for binding ribonucleotide phosphates (**P**$_n$) and bases (**B**$_n$) are indicated.

Dinucleotide and tRNA Assays. The activities (k_{cat}/K_m values) of ANG and ANG variants with dinucleotides were measured with an HPLC-based assay (*19*) using buffer B, except that for the pH study for H8A, 0.2 M sodium acetate (pH 5.0) and 0.2 M Hepes-NaOH (pH 7.0) were also used. K_i values for inhibition of ANG by nucleotides were determined with CpA as a substrate in buffer B at 25 °C as described previously (*12*). K_i values for RNase A were determined from the dependence of k_{cat}/K_m on inhibitor concentration in a spectrophotometric assay monitoring complete cleavage of CpG by 100 nM RNase A in buffer A at 37 °C (*40*). The ribonucleolytic activity of ANG toward tRNA was measured in a precipitation assay (*4*).

RESULTS AND DISCUSSION

The docking models and mutational studies presented below are described with reference to the standard nomenclature for subsites in the active site of RNase A and some specific aspects of the active site architecture in ANG (Figure 1). Therefore, we begin by briefly summarizing this information. RNases contain subsites P_n, B_n, and R_n for binding the phosphate, nucleobase, and ribose components of RNA substrates, respectively (*41*). P_1 is the subsite where cleavage of the P−O5′ bond is catalyzed by a His−Lys−His triad

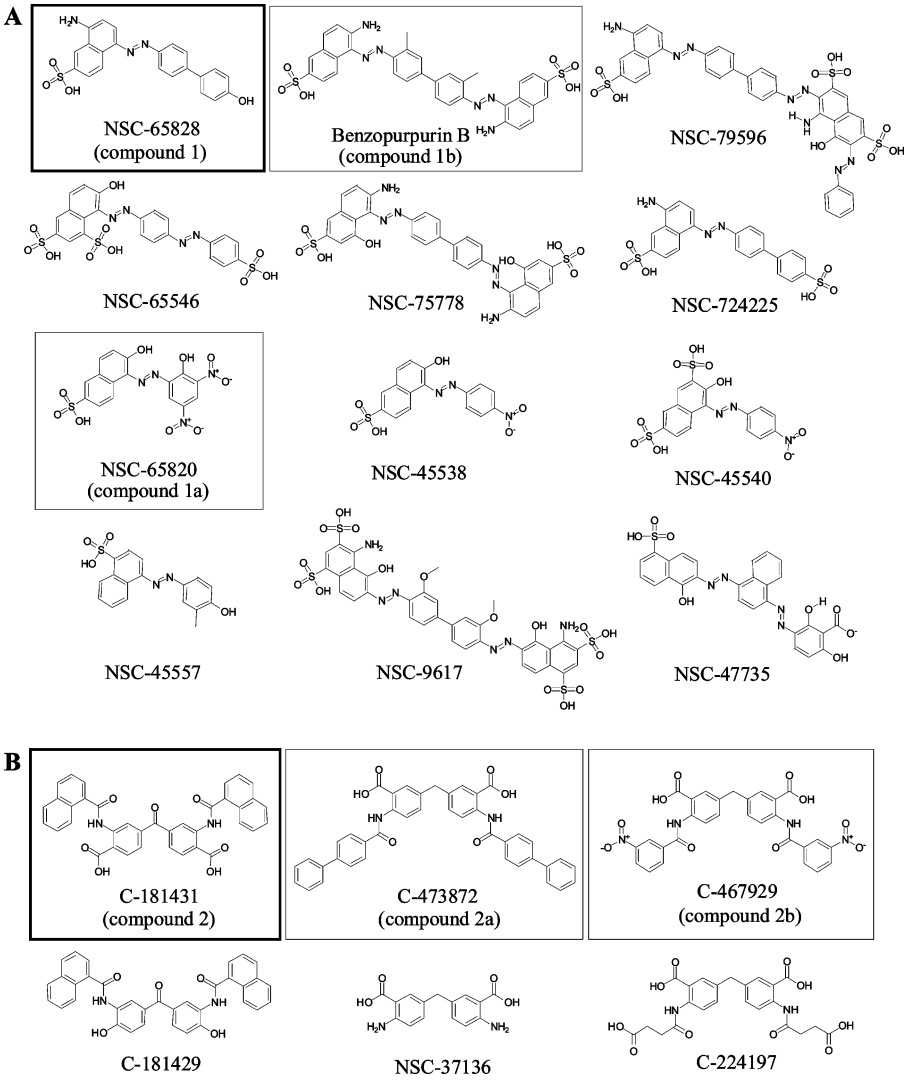

FIGURE 2: Structures of compounds **1** and **2** from HTS (boxed with thick lines) and some of the analogues that were investigated (for the complete set of compounds, see Tables 1S and 2S in the Supporting Information): (A) compound **1** series and (B) compound **2** series. The analogues selected for further study are boxed with thin lines.

[His12−Lys41−His119 in RNase A (*41*, *42*) and His13−Lys40−His114 in ANG (*6*, *7*)]. The main chain NH group of Phe120 and the side chain amide of Gln11 are also part of P_1 in RNase A (*42*), and the corresponding elements of ANG (Leu115 and Gln12, respectively) are seen to interact with phosphate in the crystal structure of the ANG−phosphate complex (*22*). B_1 is a pyrimidine-binding subsite immediately 5′ of the scissile bond. This subsite is completely open in RNase A, but is blocked by Gln117 and, to a lesser extent, the side chain of Phe120 in ANG (*21*, *43*). The obstruction, which accounts in part for the low enzymatic activity of ANG, is maintained largely by interactions of the C-terminal segment of residues 116−123, including hydrogen bonds between Asp116 and Ser118, and the hydrophobic burial of Ile119 and Phe120 (see refs *21* and *44*). Modeling indicates that rearrangement from an "inactive" (B_1-closed) to an "active" (B_1-open) conformation is required for ANG to bind and cleave RNA substrates (*28*), although the exact nature of this change remains unknown.

The B_2 subsite of ANG on the other side of the scissile bond is less developed than in RNase A, and recognition is thought to be achieved primarily through stacking interactions of the His114 imidazole (*21*); Glu108 and Asn68 also lie in or near the B_2 region in the free ANG structure, and earlier mutagenesis indicated a minor role for Glu108 (*8*). Kinetic measurements with R5A have shown that Arg5 is an important component of the P_2 subsite for binding the 5′-phosphate of the B_2/R_2 nucleoside (*19*). Modeling suggested that His8, the residue analogous to the P_2 substituent Lys7 in RNase A (*45*, *46*), may also participate in this subsite (*19*). ANG does not appear to contain an effective P_0 subsite, but a potential B_0 subsite consisting of Asp41 and/or Lys82 was proposed on the basis of modeling (*19*). Further, mutagenesis results have indicated that residues 121−123 may form a peripheral subsite on the 5′-side of the scissile bond (*29*).

*Modeling of the ANG Complexes with Compounds **1** and **2***. Compounds **1** and **2** (Figure 2) were docked onto the high-resolution crystal structure of free ANG to identify structural features likely to be important for active site recognition. Inhibitor **1** is an azo compound linking 8-aminonaphthalene-2-sulfonate with 4′-hydroxybiphenyl. All 10 docking poses were clustered within 1 Å (rmsd), indicating a strong consensus for a single binding mode. The lowest-energy pose is shown in Figure 3A. [This model was reported previously (*9*), and is described here in greater detail.] The azo group

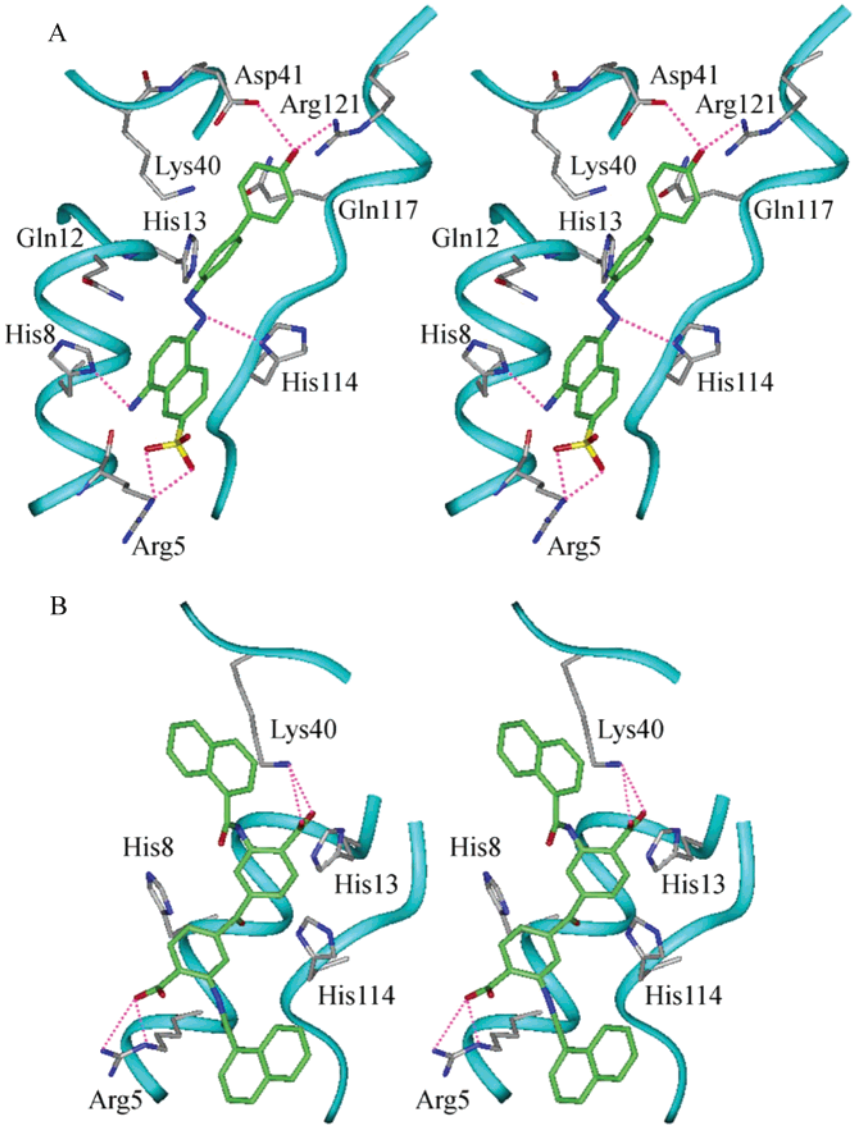

FIGURE 3: Stereoviews of lowest-energy AutoDock poses of compounds **1** (A) and **2** (B) in the ANG active site. Compounds are shown with carbon atoms in green. The backbone trace of ANG is shown, along with the side chains of residues that contact the inhibitors. Predicted hydrogen bonds are shown as dashed lines. The figure was drawn with InsightII.

is positioned in P_1, and hydrogen bonds with His114 Nδ1. One side of the naphthalene ring packs against the extended Arg5 side chain; the 2-sulfonate forms a salt bridge with the guanidino group, and the 8-amino group donates a hydrogen bond to the main chain O of this residue. The amino group also accepts a hydrogen bond from Nδ1 of His8. The phenyl proximal to the azo group is tucked between the His13 and His114 imidazoles, and the other phenyl makes hydrophobic contact with the Cα−Cγ atoms of Gln117. Both phenyl groups are positioned to form cation−π interactions (*47*) with Nζ of Lys40. Other potential contacts include hydrogen bonds between the biphenyl-OH group and Nη1 and Nη2 of Arg121 and Oδ1 of Asp41.

Compound **2** is a symmetric molecule in which two methanone-linked aminobenzoic acids are joined via amides to naphthalenecarboxylic acids. In the lowest-energy docked model, one of the benzyl carboxylates forms salt bridges with Nϵ and Nη1 of Arg5, and the other makes two with Lys40 Nζ (Figure 3B). The ketone oxygen is slightly beyond hydrogen bonding distance of the Nδ1 atoms of both His8 and His13, but small side chain adjustments would allow these interactions to form. One naphthalene lies near the putative B_2 subsite, and the other forms hydrophobic contacts with the aliphatic portion of Lys40. Three of the other nine docking poses are clustered within 2.3 Å of this model and exhibit similar interactions of the carboxylates with Arg5 and Lys40. Overall, the 10 docking poses for this compound do not cluster as well as those for compound **1**, and none are within 1 Å (rmsd) of each other.

Docking-Directed Analogue Searching and Evaluation. The models of the complexes of ANG with compounds **1** and **2** were used to guide searches of the NCI, ChemBridge, and ACD libraries for analogues. The primary objective was to identify more potent inhibitors, but some analogues were also selected to test predictions from docking regarding key substructures and to assess the contributions of specific interactions. Thus, libraries were searched both by substructure and by chemical similarity. The substructure used for compound **1** was 5-phenylazonaphthalene-2-sulfonic acid (i.e., the entire molecule except for the amino group and the benzyl alcohol), whereas for compound **2**, we used only the core consisting of the linked benzoic acids, whose

carboxylates appear to form the major anchoring contacts at P_1 and P_2 in the model.

Searching of the NCI library for compound **1** analogues by substructure and by similarity (85% with respect to the full structure) yielded 102 and 99 analogues, respectively, with 29 common to the two hit lists. The structures of these 172 compounds were inspected manually, and 49 were selected for testing; 31 incorporated the query substructure. The substructure and similarity searches of the ACD library gave 23 and 179 compounds, respectively. Six of these were manually chosen for testing, and another six after prioritization by high-throughput docking. All but one contain the substructure. The ChemBridge library contained no analogues that met either search criterion.

The K_i values of the 61 analogues of compound **1** that were evaluated were found to range from 27-fold lower to >10-fold higher than that of the original inhibitor. (Tables S1 and S2 in the Supporting Information list the structures and K_i values of all compound **1** and **2** analogues that were tested; the structures of the compounds cited below are also shown in Figure 2.) Sixteen analogues are at least 2-fold more effective than compound **1** ($K_i = 3-38$ μM vs 81 μM). Most of these are bis-azo or tris-azo compounds that are considerably larger than compound **1** (e.g., benzopurpurin B and NSC-79596), suggesting that inhibitor components that extend farther than the hydroxybiphenyl of compound **1** can form productive interactions with ANG. Eight other bis- or tris-azo analogues that contain the substructure (e.g., NSC-65546 and -75778) have lower inhibitory potency than compound **1**. Although the compound **1** docking pose had indicated a potential clash of most multiazo analogues with the C-terminal tripeptide of ANG, we did not eliminate these compounds from consideration because this region is not well-ordered in the ANG crystal structure. Moreover, as noted above, the C-terminal segment is postulated to undergo a major conformational change to accommodate substrates, and we thought it was possible that some restructuring could also occur when inhibitors bind.

Despite the relatively high number of compound **1** analogues that were examined, there are only a few instances in which variations are sufficiently small that structure−activity relationships can be established. Substitution of the hydroxyl group of compound **1** with a sulfonate (NSC-724225) has no impact on affinity. Benzopurpurin B binds to ANG 35-fold more tightly than does NSC-75778, which is structurally identical except that its two naphthalene rings contain additional 4-hydroxyl groups and its central biphenyl lacks two methyl groups. NSC-65820 is 12-fold more potent than NSC-45538, which differs only in its phenyl substituents (two nitro groups and an OH group for NSC-65820 vs a single nitro group for NSC-45538). Addition of a 7-sulfonate to NSC-45538 (generating NSC-45540) has no effect on affinity. Although structural differences in most other cases are more substantial, some general conclusions seem to be warranted. (i) The putative critical substructure is indeed important. Only one of the top 20 compounds does not contain it, as compared to 12 of the bottom 20. (ii) In particular, a sulfonate at the naphthalene 2-position in 5-azo compounds is highly advantageous (as is evident, e.g., from the poor inhibition by NSC-45557, which has a sulfonate at the 8-position rather than the 2-position). (iii) Shifting of the azo from the 5- to 6-position on the naphthalene is well-tolerated if the 2-sulfonate is simultaneously moved to the 3-position (e.g., as in NSC-9617 and -47735), maintaining similar spacing between the two groups. (iv) Affinities do not correlate with the number of negative charged groups (which ranges from 0 to 4, primarily sulfonates). This finding is noteworthy in view of the cationic character of the ANG active site, and its potential for nonspecific binding based on ion exchange.

Searching of the ChemBridge library for compound **2** analogues containing the methanone-linked dibenzoic acid core yielded 11 hits, whereas 99 were obtained with a search criterion of 90% chemical similarity to this substructure. Most of the latter were found to differ from compound **2** in that the positions of the carboxyl and amino substituents on the core phenyl groups are reversed; i.e., these groups are *meta* and *para*, respectively, vis-à-vis the bridge rather than *para* and *meta*, respectively. The bridge in all such compounds is a methylene group rather than a methanone. In these analogues, the two *m*-carboxylates are separated by a distance similar to that of the *p*-carboxylates in compound **2**. Therefore, an additional search based on this substructure was performed, yielding 50 compounds. Eight of these were selected manually for testing, along with two of the analogues that have the compound **2** substructure. Four additional candidates were selected by high-throughput docking of the hit list from the similarity search (three other compounds that ranked highly had already been included from the substructure search). Searches of the NCI and ACD libraries yielded only 2 compounds, both from NCI; these were also included in the set for evaluation.

The 16 analogues of compound **2** that were tested had K_i values ranging from 2-fold lower to >10-fold higher than that of compound **2** itself. Only two were more effective (C-473872 and -467929, with K_i values of 20 and 24 μM, respectively, vs 41 μM for compound **2**). C-181429, in which the carboxylates of compound **2** are replaced with hydroxyls, gave no detectable inhibition, indicating that these carboxylates are indeed critical, and neither did NSC-37136, a compound with *m*-carboxylates and underivatized amino groups. Thus, one or both of the groups with an amide linkage to the amines are also important. C-224197, in which these groups are short alkyl acids rather than aromatic rings, also did not inhibit ANG at the highest concentration that was tested.

Two analogues of compound **1** (NSC-65820 and benzopurpurin B, hereafter designated compounds **1a** and **1b**, respectively) and two analogues of compound **2** (C-473872 and C-467929, designated compounds **2a** and **2b**, respectively) were selected for further characterization. K_i determinations (Table 1) were carried out in both the HTS buffer (*9*) and the buffer used in previous nucleotide inhibition studies so that direct comparisons could be made (e.g., see ref *20*). Compound **1a** was chosen because it is the most effective mono-azo inhibitor ($K_i = 25$ μM). It contains 6-hydroxynaphthalene-2-sulfonate with a 5-azo linkage to 2-hydroxy-3,5-dinitrophenyl. Compound **1b** is a symmetrical bisulfonated bis-azo compound and is the smallest of the group of inhibitors with the lowest K_i values (3−5 μM). As already noted, compounds **2a** and **2b** are the only compound **2** analogues that bind more tightly. Both have the alternative (*m*-carboxylate) core and are symmetrical; in compound **2a**, the groups with an amide linkage to the core are biphenyl-

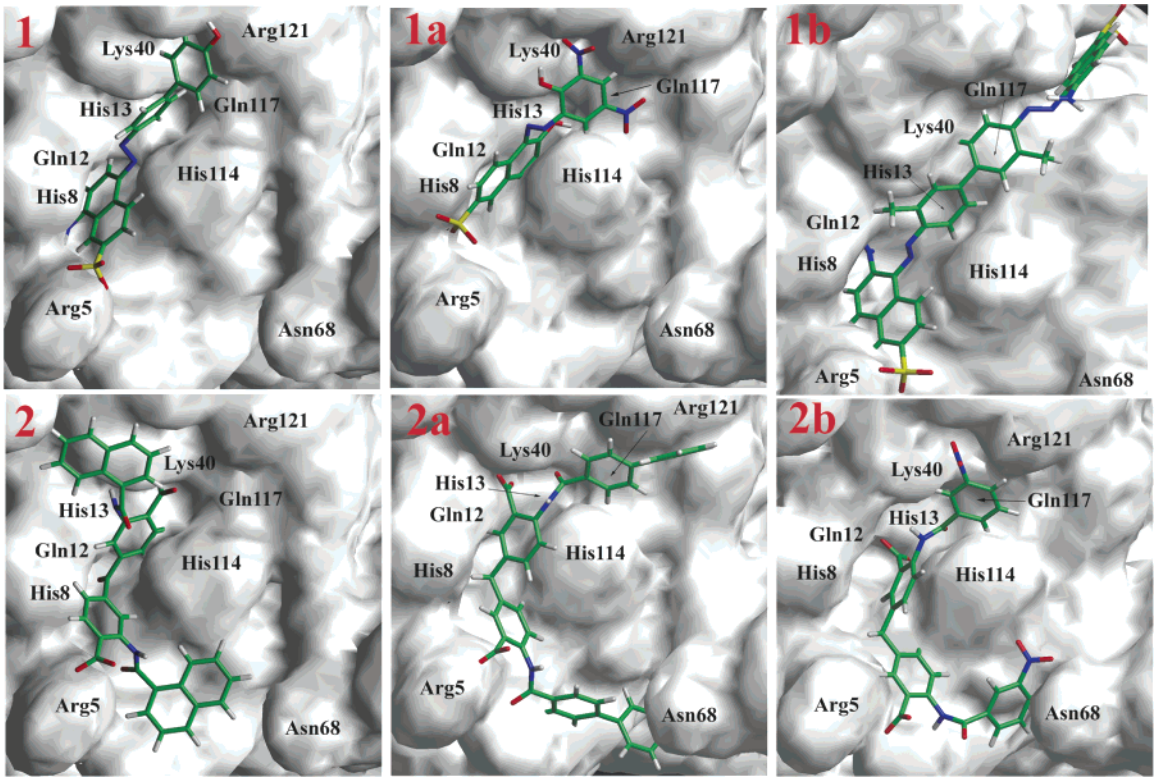

FIGURE 4: Binding orientations of compounds **1**, **1a**, **1b**, **2**, **2a**, and **2b** (stick rendering) predicted by the AutoDock Lamarckian Genetic Algorithm. ANG (PDB entry 1B1I) is shown as a surface model. For the compound **1b** model, ANG residues 119−123 were deleted (see the text).

Table 1: Compound K_i Values

			K_i (μM)	
compound	name	MW	buffer A[a]	buffer B[b]
1	NSC-65828	420	81 ± 3[c]	58 ± 2
1a	NSC-65820	434	25 ± 1	18 ± 2
1b	benzopurpurin B	681	5.0 ± 0.2	4.7 ± 0.4
2	C-181431	609	41 ± 2[c]	12 ± 1
2a	C-473872	649	20 ± 1	22 ± 1
2b	C-467929	586	24 ± 1	7.0 ± 0.2

[a] Assay conditions: 20 mM Hepes-NaOH and 100 mM NaCl, pH 7.0, at 37 °C. [b] Assay conditions: 200 mM Mes-NaOH, pH 5.9, at 25 °C. [c] From ref *9*.

carboxylic acids, whereas in compound **2b**, they are nitrobenzenecarboxylic acids. Overall, the docking-directed search for available analogues of the HTS-generated hits resulted in improvements in K_i of 3−16-fold for the compound **1** series and of ∼2-fold for the compound **2** series, as measured in HTS buffer. These K_i values are 20−160-fold lower than that for the most effective nucleotide inhibitor of ANG, 5′-diphosphoadenosine 2′-phosphate, under these conditions [500 μM (*9*)]. The K_i values for the six non-nucleotides in the standard assay for nucleotide inhibitors were either similar to (**1b** and **2a**) or lower than (up to 3.4-fold, **2** and **2b**) those under the HTS conditions, and up to ∼20-fold below the value for 5′-diphosphoadenosine 2′-phosphate (*19*).

*Modeling of ANG−Analogue Complexes. (i) Compound **1a***. The lowest-energy docking pose for compound **1a** is generally similar to that of compound **1**, but the naphthalene-azo portion is shifted 1−2 Å and rotated slightly (Figure 4). The interaction of the azo group and His114 Nδ1 is retained, along with the salt bridge between the 2-sulfonate and the Arg5 guanidino group. The naphthalene 6-OH group not present in compound **1** is positioned to form hydrogen bonds with both the O and NH group of the Leu115 backbone. The 2-hydroxy-3,5-dinitrophenyl moiety occupies a space largely different from that of the hydroxybiphenyl of compound **1**, and all three of its functional groups hydrogen bond with ANG: the 2-OH and 3-NO_2 groups both hydrogen bond to Lys40, and the 5-NO_2 group is within range of the main chain NH group of Gln117. Overall, the hydrogen bonding contribution in this pose is somewhat greater than that of compound **1**. Seven of the other nine docking poses for compound **1a** clustered within 2 Å of the lowest-energy model.

*(ii) Compound **1b***. Docking of the bis-azo compound **1b** to ANG resulted in poorly fitting configurations with predicted binding energies well above experimentally determined values. This was not unexpected in view of the conflict involving the C-terminal residues in the crystal structure of ANG discussed above. When residues 119−123 were removed, compound **1b** was able to dock in a manner strikingly similar to that of compound **1** (Figure 4), with the positions of the biphenyl group and the "lower" naphthalene and azo groups all within ∼1 Å of those in the original inhibitor. The 2-sulfonate still forms a salt link with Arg5, but His114 is now beyond hydrogen bonding range of the azo nitrogens. The 6-NH_2 group donates a hydrogen bond to Oϵ1 of Gln12 and accepts one from Nϵ2 of His13. The additional naphthalene ring forms hydrophobic contacts with the side chain of Ile42, and its sulfonate makes two salt links with Nζ of Lys82. The amino substituent of this naphthalene and the second azo group do not interact with ANG. All nine of the other docking poses clustered within 2 Å of the top-ranking pose.

*(iii) Compound **2a***. In the lowest-energy docking pose, compound **2a** arcs in a semicircular fashion around His114 (Figure 4). Although a high intramolecular ligand energy was calculated for achieving this configuration (11.4 kcal/mol), it was counterbalanced in the overall energy score by intermolecular contacts. The core structure of linked benzoic acids occupies a space similar to that of compound **2** in its model complex, and again forms hydrogen bonds with Arg5 and Lys40, but there are some notable differences in ring orientations. The "lower" carboxylate lies only ∼1 Å from its position in the compound **2** model and forms the same interactions with Arg5. However, the "upper" carboxylate is shifted by almost 3 Å and replicates only one of the two hydrogen bonds with Lys40 while forming an additional interaction with Nϵ2 of Gln12. The oxygen of the upper amide of compound **2a** also hydrogen bonds with Nζ of Lys40. The first ring of the lower biphenyl partially superimposes with the corresponding part of the naphthalene group of compound **2**, but the distal phenyl ring travels into a different region, where it tucks in behind the side chain of Asn68. The upper biphenyl is oriented in a manner quite different from that of the upper naphthalene of compound **2** and lies near the aliphatic portions of the Gln117 and Arg121 side chains. As with compound **2**, there is little clustering of the 10 docking poses, although six of them show the predicted key interactions of the benzoic acids with Arg5 and Lys40.

*(iv) Compound **2b***. Compound **2b** adopts a semicircular conformation similar to that of compound **2a** in its lowest-energy pose, but its core is shifted by a few angstroms (Figure 4). The upper carboxylate is deeper in the P_1 subsite, in position to hydrogen bond with Nϵ2 of His13 and the main chain NH group of Leu115 rather than Nζ of Lys40. The upper amide oxygen is also positioned to interact with His13 and the Leu115 NH group instead of Lys40. The lower carboxylate is slightly beyond hydrogen bonding distance of the guanidino group of Arg5, but a minor rotation of the amino acid side chain would be sufficient to reestablish this interaction. The upper phenyl partially superimposes with that of the corresponding group of compound **2a**, and its nitro group accepts hydrogen bonds from Lys40 Nζ and Arg121 Nη2. The lower phenyl is packed against the side chains of Asn68, Leu69, and Ala106, and its nitro group accepts a hydrogen bond from Nδ2 of Asn68. Again the various docking poses did not cluster well, and only three were within 3 Å of the lowest-energy pose.

(v) Comparison of Predicted and Observed Free Energies of Binding. The binding energies for the inhibitors calculated by AutoDock followed the same order as the values determined experimentally, except that compound **1** was ranked too high (second rather than sixth). All of the predicted binding energies (from −8.1 to −12.2 kcal/mol) were at least 1.7 kcal/mol lower than the observed values (from −5.8 to −7.5 kcal/mol). In three cases (compounds **1a**, **2a**, and **2b**), the discrepancy fell within the intrinsic standard error of 2.2 kcal/mol estimated for AutoDock (*26*). The largest difference (4.7 kcal/mol) was with compound **1b**, where the receptor used for docking had been truncated at the C-terminus to avert a possible clash, as discussed above. In contrast, docking to the full ANG structure yielded a poor calculated binding energy, much less favorable than the experimental value. These findings suggest that the predicted binding mode of compound **1b** is generally correct, and that the large gap between the calculated and actual binding energies reflects a penalty associated with conformational adjustments of ANG. The more modest disparities for the other compounds might result from differences in buffer conditions or inhibitor characteristics as compared to those used to calibrate the AutoDock binding free energy function. With regard to the latter, we note that the inhibitors used to calibrate AutoDock for K_i values above 10 μM contained only 5−18 non-hydrogen atoms for inhibitors, whereas our compounds in the same affinity range contained 30−49 atoms. It is also possible that some of the ANG residues in the ligand binding site (e.g., Arg5 and Arg121) are more flexible than for the AutoDock calibration set, and that the contributions of their interactions are therefore overestimated.

Table 2: Enzymatic Activities of ANG and ANG Variants[a]

	$(dA)_5rC(dA)_2$		CpA
enzyme	k_{cat}/K_m (M^{-1} s^{-1})	$(k_{cat}/K_m)_{wt}/(k_{cat}/K_m)_{var}$	$(k_{cat}/K_m)_{wt}/(k_{cat}/K_m)_{var}$
ANG[b]	336 ± 14		
R5A[b]	33 ± 5	10.2	1.7[d]
H8A[b]	88 ± 3	3.8	6.2
Q12A[b]	325 ± 7	1.0	1.0
N68A[b]	269 ± 4	1.2	2.1
des(121−123)[b]	77 ± 3	4.4	1.4[e]
ANG[c]	27 ± 1[f]		
Q117G[c]	974 ± 67	0.03	0.04[g]

[a] Activities were determined as described in Experimental Procedures. [b] Kinetic assays performed in 200 mM Mes-NaOH, pH 5.9, at 25 °C. [c] Kinetic assays performed in 20 mM Hepes-NaOH and 100 mM NaCl, pH 7.0, at 37 °C for $(dA)_5rC(dA)_2$ and in 200 mM Mes-NaOH, pH 5.9, at 25 °C for CpA. [d] From ref *27*. [e] From ref *29*. [f] From ref *9*. [g] From ref *28*.

Effects of ANG Active Site Mutations on Inhibitor Binding. Inhibition studies were performed with active site variants of ANG to further characterize ANG−ligand binding interactions and to assess the validity of the model complexes generated by docking. Many variants were available from earlier studies (*6*−*8*, *12*, *27*−*30*, *48*). Six of them containing substitutions or deletions of residues that form intermolecular contacts in one or more of the models were selected for testing: R5A, H8A, Q12A, N68A, Q117G, and des(121−123) (in which the C-terminal Arg121-Arg122-Pro123 tripeptide has been deleted). The enzymatic properties of H8A, Q12A, and N68A (*30*) had not been characterized previously, and are reported here. Although the catalytic triad variants H13A, H114A, and K40G (*7*, *30*) would also have been of interest, measurement of inhibitor binding to these enzymatically inactive proteins would require the use of physical methods, which have thus far not proven to be feasible. K_i values were determined by using HPLC-based inhibition assays as for wild-type ANG. Activities of the six variants with the octameric substrate $(dA)_5rC(dA)_2$ and the dinucleotide CpA are provided in Table 2, and the effects of the mutations on inhibitor potency are shown in Figure 5 and in Table S3 of the Supporting Information. The data for the R5A variant with compound **1** were reported previously (*9*). The supply of compound **2** was limited, and measurements for this inhibitor were performed only with R5A and H8A.

(i) R5A. Replacement of Arg5 with Ala was shown previously to produce a smaller decrease in activity toward

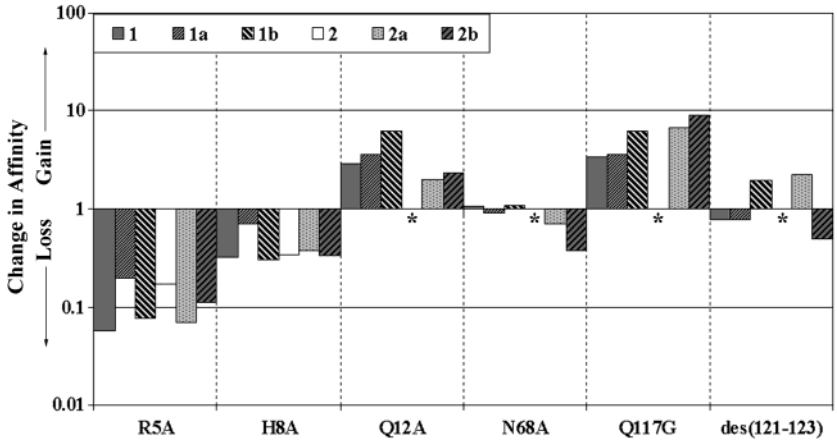

FIGURE 5: Changes in the affinity of inhibitors for ANG variants as compared to that of wild-type ANG, determined in HPLC-based enzymatic assays. Changes in affinity were calculated as $K_{i,wild-type}/K_{i,variant}$. Asterisks for compound **2** with Q12A, N68A, Q117G, and des(121−123) indicate that measurements were not performed (see the text).

CpA than toward tRNA and CpAp, indicating a role for Arg5 in the P_2 subsite (*19*, *27*). With $(dA)_5rC(dA)_2$, this substitution reduces k_{cat}/K_m by 1 order of magnitude. Binding of all six inhibitors was also weakened appreciably (from 5- to >17-fold, Figure 5), consistent with the presence of hydrogen bonds of the Arg5 guanidino group with a sulfonate or carboxylate as predicted by the AutoDock models. The largest change was seen for compound **1**, which appears to form particularly favorable interactions with Arg5 in the model complex.

(ii) H8A. Replacement of His8 with Ala reduces activity toward all substrates, and these effects are no greater for large substrates [10-fold for tRNA and 4-fold for $(dA)_5rC(dA)_2$] than for dinucleotides (6-fold for CpA and 10-fold for CpG, CpC, and UpA) or even the minimal substrate cytidine cyclic 2′,3′-phosphate (16-fold). This indicates that His8 influences the function of the P_1 or B_1 subsite rather than P_2, as had been hypothesized on the basis of the location of this residue in the ANG crystal structure. Analogous results were reported for replacement of the corresponding residue of RNase A, Lys7 (*46*), whose role in P_2 has been directly demonstrated in crystal structures of complexes with nucleotides (*45*). It was proposed that Lys7 enhances the efficiency of P_1 through long-range Coulombic interactions that depress the pK_a values of catalytic residues His12 and His119 (*49*). However, Coulombic effects on P_1 are unlikely to account for the reduced activity of H8A; the changes in k_{cat}/K_m values for CpA cleavage are nearly identical over a range of pH values [5.0 (6.0-fold), 5.9 (6.0-fold), and 7.0 (6.9-fold)] spanning the pK_a of His8 [6.5 (*50*)], and therefore appear to be independent of the protonation state of this residue.

Inhibition of H8A by compounds **1**, **1b**, **2**, **2a**, and **2b** was ∼3-fold weaker than with ANG, whereas binding of compound **1a** was barely affected by the amino acid replacement (Figure 5). As noted above, the His8 imidazole forms hydrogen bonds with compounds **1** and **1b** in the AutoDock models; rotation of this residue would allow hydrogen bonds with compounds **2** and **2b** as well. Although His8 does not hydrogen bond with compound **2a** in the model, it does partially shield the bridge from solvent (Figure 4). For compound **1a**, neither function appears to be served. Thus, the experimental findings are reasonably consistent with the models overall. At the same time, it may not be a coincidence that the losses in affinity for nearly all of the inhibitors are similar in magnitude to the (as yet unexplained) decrease in ribonucleolytic activity with this variant. Whatever feature of His8 underlies the effect of the Ala substitution on enzymatic activity may also be responsible for the changes in inhibitor potency.

(iii) Q12A. Replacement of the P_1 subsite residue Gln12 with Ala had little effect on k_{cat}/K_m values for cleavage of $(dA)_5rC(dA)_2$ or any of the dinucleotides that were tested. [Activities relative to that of ANG are 1.0 for the octanucleotide (Table 2), 1.0 for CpA, 1.0 for CpG, 0.77 for UpA, and 1.2 for CpC.] These findings are similar to those reported for substitution of the analogous residue of RNase A, Gln11 (*51*), where relatively minor changes in k_{cat}/K_m values for cleavage of poly(C) and UpA were measured. For RNase A, more detailed kinetic analysis showed that there were larger, approximately equal decreases in both k_{cat} and K_m, and it was proposed that the function of Gln11 is to prevent nonproductive binding of substrate. For ANG, determination of individual k_{cat} and K_m values is difficult because of extremely weak binding by substrate (*28*). Therefore, we used a nucleotide inhibitor to assess the impact of the Gln12 to Ala replacement on binding. The K_i value of 2′-CMP was found to be 3.9-fold lower with Q12A than with wild-type ANG (1.4 vs 5.4 mM), paralleling the K_m effect seen with the Q11A−RNase A complex.

Binding of the non-nucleotide inhibitors to Q12A is also tighter than binding to ANG; K_i differences range from 2-(compound **2a**) to 6-fold (compound **1b**) (Figure 5). Thus, Gln12 appears to impede binding of these compounds as well, although most of the AutoDock models show some favorable interactions for this residue. The models of the compound **1b** and **2a** complexes in particular include short hydrogen bonds with Gln12. It is possible that removal of the Gln12 side chain causes structural rearrangements that simultaneously improve binding of both nucleotide and non-nucleotide inhibitors to the ANG active site. For example, the neighboring residues His8 and Lys40 might move into more advantageous positions for binding. The orientation of the His8 imidazole seems to be partially fixed by a hydrogen bond with Oϵ1 of Gln12, and that of Nζ of Lys40 might be influenced by the proximity of the Gln12 side chain amide as well.

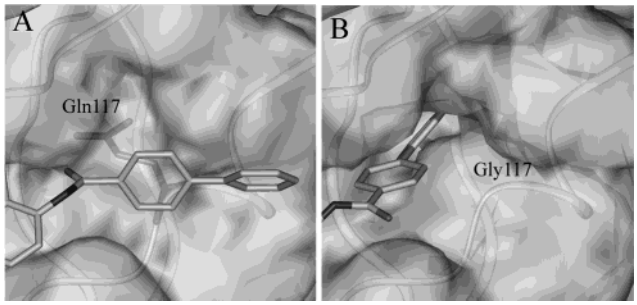

FIGURE 6: Comparison of docking modes for the upper biphenyl group of compound **2a** (see Figure 4) with ANG (A) and Q117G (B), as predicted by AutoDock. The protein surface and backbone trace along with the side chain of Gln117 are shown (50% transparent). This figure was generated with InsightII.

(iv) N68A. Replacement of Asn68 with Ala resulted in small decreases in activity toward dinucleotides: 2.1-fold for CpA, 2.9-fold for UpA, 1.1-fold for CpG, and 1.5-fold for CpC. The magnitude of the changes was dependent on the identity of the base occupying site B_2, suggesting that Asn68 plays a minor role in this subsite. Activity toward $(dA)_5rC(dA)_2$ was 80% of that for ANG (Table 2). The replacement had no effect on inhibition by the compound **1** series (Figure 5), consistent with the AutoDock models (Figure 4), in which Asn68 does not approach any of these inhibitors. Binding of compound **2b**, which forms a hydrogen bond with Asn68 in the model complex, was weakened by 2.7-fold, whereas that of compound **2a**, which makes only van der Waals contacts with this residue, was weakened by 1.4-fold.

(v) Q117G. Substitution of the B_1-obstructing residue Gln117 with Gly was shown previously to increase activity toward dinucleotides by 21−29-fold, reflecting ∼5-fold improvements in both k_{cat} and K_m (*28*). We find that activity toward $(dA)_5rC(dA)_2$ is enhanced by 36-fold (Table 2). In the AutoDock models of the ANG complexes with compounds **1**, **1a**, **1b**, **2a**, and **2b**, the Gln117 Cβ−Cγ atoms seem to form favorable hydrophobic contacts with one of the phenyl rings of each compound (Figure 4). Nonetheless, all of the inhibitors bound more tightly to Q117G than to ANG, by factors of 3.2, 3.5, 6.1, 6.7, and 9.2, respectively (Figure 5). To explore possible physical bases for these affinity increases, we docked compounds **1**, **1a**, **2a**, and **2b** to the high-resolution crystal structure of Q117G (*44*). This structure shows no major changes other than the loss of the position 117 side chain, which creates a cavity in the B_1 region. In all of the Q117G AutoDock complexes, the inhibitor exploits this new feature. This is most striking for compound **2a**, where the upper biphenyl group (Figure 4) travels in a direction different from that in the ANG model and becomes largely buried in the putative B_1 site formed by Thr44, Ile42, and Phe120 (Figure 6) (*21*). Outside of this region, the docking poses for this inhibitor and the others are largely unchanged. The binding energy scores calculated by AutoDock for the Q117G models with all four inhibitors are superior to those for the wild-type ANG models (Table 3).

(vi) Des(121−123). It was shown earlier that deletion of the C-terminal tripeptide of ANG has only a minor effect on k_{cat}/K_m values with dinucleotides, but decreases activity toward polynucleotide substrates by 10-fold (*29*). On this basis, it was proposed that residues 121−123 contribute to a peripheral binding subsite, probably B_0. The crystal structure of des(121−123) subsequently raised an alternative possibility, i.e., that a perturbation of the side chain of Lys82, which was previously cited as a B_0 subsite candidate (*19*), underlies the reduction in activity toward large substrates (*44*). With the substrate $(dA)_5rC(dA)_2$ used for our inhibition studies, des(121−123) is 4.4-fold less efficient than wild-type ANG (Table 2).

Table 3: Comparison of AutoDock Binding Energy Scores for Complexes of Wild-Type ANG and Q117G[a]

compound	$\Delta G_{wild-type}$ (kcal/mol)	ΔG_{Q117G} (kcal/mol)	$\Delta\Delta G^b$ (kcal/mol)
1	−9.69	−10.24	−0.55
1a	−8.19	−8.93	−0.74
2a	−9.14	−11.61	−2.47
2b	−8.59	−9.56	−0.97

[a] Calculation of binding energy scores is discussed in Experimental Procedures. [b] $\Delta G_{Q117G} - \Delta G_{wild-type}$.

Deletion of residues 121−123 affected binding of the various inhibitors in diverse ways. Losses in affinity of up to 2-fold were observed for compounds **1**, **1a**, and **2b**, whereas ∼2-fold increases were seen for compounds **1b** and **2a** (Figure 5). The direction of the change correlates well with the size of the compound components that extend toward the ANG C-terminus in the AutoDock models. As discussed above, if the binding mode of compound **1b** were analogous to that predicted for compound **1**, the extra azonaphthalenesulfonate moiety would bump against the C-terminal tripeptide of ANG. Repositioning of this flexible ANG segment to avoid the clash would presumably have an energetic cost, perhaps explaining the greater affinity of compound **1b** for des(121−123). The other compound that binds more tightly to the deletion variant, **2a**, also contains a large substituted naphthalene group in the corresponding region, and removal of residues 121−123 might provide access to a binding surface for this moiety that is preferred over the one in the native structure. Moreover, Arg121 is the primary component of ANG that forces compound **2a** into its strained semicircular conformation in the AutoDock model, and deletion of this residue would allow the inhibitor to adopt a lower-energy conformation. The smaller compounds (**1**, **1a**, and **2b**) that have lower affinities for des(121−123) appear to make more favorable interactions with Arg121 in the AutoDock models: the compound **1** hydroxyl and compound **2b** nitro group are within hydrogen bonding distance of the Arg121 guanidino, and a minor side chain rotation would allow the formation of a hydrogen bond with the 3-nitro group of compound **1a**.

Effect of Salt Concentration on Inhibition. ANG and RNase A become enzymatically less active and bind nucleotide inhibitors less tightly as the salt concentration is increased, reflecting the weakening or disruption of interactions between substrate phosphates and cationic active site residues (*37*, *52*, *53*). The influence of salt concentration on the affinity of ANG for the six non-nucleotide inhibitors was examined to assess the importance of ionic interactions in the complexes of ANG with these compounds and to further test the docking models. The activity of ANG toward $(dA)_5rC(dA)_2$ decreased from 1230 ± 72 to 142 ± 5 and 34 ± 1.5 M^{-1} s^{-1} as the Na^+ concentration was increased from 26 to 106 and 206 mM, respectively. The K_i values for all five compounds that were examined were below 10 μM when

Table 4: Effect of Salt Concentration on Compound K_i Values (μM)[a]

compound	26 mM Na^+ [b]	106 mM Na^+ [c]	206 mM Na^+ [d]
1	9.4 ± 0.2 (**1**)	63 ± 1 (**6.7**)	—[e]
1a	6.2 ± 0.3 (**1**)	16 ± 3 (**2.6**)	31 ± 2 (**5.0**)
1b	1.3 ± 0.2 (**1**)	4.4 ± 0.7 (**3.4**)	24 ± 5 (**18**)
2a	4.3 ± 0.3 (**1**)	20 ± 1 (**4.7**)	40 ± 5 (**9.4**)
2b	3.1 ± 0.5 (**1**)	8.3 ± 0.4 (**2.7**)	28 ± 1 (**9.0**)

[a] Values were determined as described in Experimental Procedures. The fold increases in K_i relative to the lowest Na^+ concentration are shown in bold. [b] Assay conditions: 20 mM Mes-NaOH and 20 mM NaCl, pH 5.9, at 37 °C. [c] Assay conditions: 20 mM Mes-NaOH and 100 mM NaCl, pH 5.9, at 37 °C. [d] Assay conditions: 20 mM Mes-NaOH and 200 mM NaCl, pH 5.9, at 37 °C. [e] Value could not be determined due to precipitation of the compound.

Table 5: Inhibition of RNase A[a]

compound	K_i (μM)	$(K_i)_{RNase}/(K_i)_{ANG}$[b]
1	24 ± 5	0.3
1a	38 ± 1	1.5
1b	2.5 ± 0.7	0.5
2	19 ± 5	0.5
2a	45 ± 2	2.3
2b	21 ± 1	0.9

[a] K_i values were determined as described in Experimental Procedures. Assays were carried out in 20 mM Hepes-NaOH and 100 mM NaCl, pH 7.0, at 37 °C. [b] K_i values for ANG are from Table 1 (buffer A).

the lowest Na^+ concentration was used (Table 4). For compounds **2a** and **2b**, K_i values were ~9-fold higher in the buffer containing 206 mM Na^+, whereas increases of 5- and 18-fold were observed for compounds **1a** and **1b** (no value could be measured for compound **1** at high Na^+ concentrations because of poor solubility). Moreover, log−log plots of K_i versus Na^+ concentration either are linear (compounds **1a** and **2a**) or reveal greater changes as the Na^+ concentration increases (not shown). Thus, ionic contacts play a major role in recognition of these inhibitors.

Specificity of Inhibitors for ANG versus RNase A. Humans have seven RNase homologues of ANG (see refs *54* and *55*), including a pancreatic-type RNase whose active site structure is essentially identical to that of RNase A (*56*). A recent report (*57*) suggests that human pancreatic RNase may have a role in vascular homeostasis apart from its digestive function. RNase 2 and RNase 3 (also known as eosinophil-derived neurotoxin and eosinophil cationic protein, respectively) are thought to participate in host defense (*58*), and it has been proposed that RNase 4 also has a nondigestive role (*59*). Thus, it may be necessary for ANG inhibitors that are used clinically to have a strong preference for ANG over its relatives. It was therefore of interest to characterize the specificity of the present non-nucleotide compounds. All small nucleotide inhibitors examined to date bind much more tightly to RNase A and related human RNases than to ANG. K_i values for ANG are typically >100-fold higher than for the other enzymes (*19*, *20*), although one nucleotide ($NADP^+$) was recently shown to bind to ANG only ~6-fold less tightly than to RNase A (*60*).

We find that the K_i values for compounds **1a** and **2a** are 1.5- and 2.3-fold lower for ANG than for RNase A (Table 5), respectively, making these the first small molecules that have been shown to exhibit any preference for ANG. Compound **2b** binds to the two enzymes with similar affinities, whereas compounds **1**, **1b**, and **2** are somewhat (2−3.4-fold) more effective against RNase A. The basis for these experimental observations was explored by modeling. For the most ANG-specific inhibitor, compound **2a**, superposition of the crystal structure of RNase A onto the AutoDock model of the ANG complex showed clashes between the lower biphenyl group (Figure 4) and B_2 residues Gln69 and Asn71 of RNase A (whereas this biphenyl fits well into the more expansive space in the ANG B_2 subsite behind Asn68). Docking of compound **2a** to the RNase A structure in AutoDock places the biphenyl in a different region, between the N-terminal α-helix and residues 111−113 on the $\beta6-\beta7$ loop. In the lowest-energy pose, the upper biphenyl enters the open B_1 site, but only one of the carboxylates forms interactions (with Gln11 and Lys7). In an alternate pose where the two carboxylates occupy the P_1 and P_2 subsites, the biphenyls are unable to go into the B_1 or B_2 site. The AutoDock models of the other five compounds with RNase A also show binding modes different from those for ANG. For example, the sulfonate of compound **1a** is positioned in P_1 rather than P_2, and the 2-hydroxy-3,5-dinitrophenyl occupies the B_2 site rather than extending into the P_1-B_1 region.

Conclusions and Implications. The new ANG inhibitors identified here have greater in vitro potency than any previous small-molecule antagonists. The K_i values for the most effective of these compounds are in the low-micromolar range under near-physiological conditions, up to 20-fold below those of the inhibitors we had obtained by HTS and as much as 160-fold lower than that of the best nucleotide antagonist. All of the non-nucleotides examined in detail have more favorable selectivity for ANG versus RNase A than do the nucleotides originally investigated as ANG inhibitors (*20*). Further optimization of both affinity and specificity will most likely be required for pharmacological efficacy in humans while averting untoward side effects. However, the magnitudes of these improvements are unclear at this stage. The amount of endogenous ANG in the human body is relatively large [normal plasma contains ~25 nM ANG (*61*, *62*)], and it will therefore be necessary to achieve fairly high concentrations of inhibitor in vivo. Thus, there may be no major advantage in lowering the K_i value beyond the mid-nanomolar range. In this regard, it should be noted that even compound **1**, with a K_i of 81 μM, was able to retard or prevent the establishment of human tumor xenografts in athymic mice when administered locally at modest doses (*9*). The degree of selectivity vis-à-vis ANG homologues that will be required depends on the importance of these other enzymes in normal physiological processes, which is as yet unknown.

The computational models of ANG−inhibitor complexes constructed here should provide a rational basis for designing more potent and specific antagonists. These models are highly consistent with the results obtained with compound analogues and ANG variants, as well as with comparisons of inhibitor avidity for ANG versus RNase A. The effects of the active site mutations perhaps provide the strongest support. All of the models exhibit strong interactions of inhibitor sulfonate or carboxylate groups with Arg5, and Ala replacement indeed decreases affinity markedly for every one of the compounds. His8 is predicted to contact all of the compounds except for **1a**, and this inhibitor was the only

one whose binding was not significantly weakened in H8A. Asn68 contacts only compounds **2a** and **2b** in the models, and these are the only inhibitors whose affinity is diminished by Ala substitution. The largest compound, **1b**, was expected to bump against the C-terminal tripeptide of ANG, and deletion of these residues was found to increase the avidity for this inhibitor, but not for smaller compounds **1**, **1a**, and **2b**. Although it was not apparent from the models that removal of the Gln117 side chain would enhance binding of the five inhibitors that were examined, the AutoDock calculations for these models predicted that this would be the case. The only results for which the docking models could not account were the universal decreases in K_i produced by the Gln12 to Ala replacement. In this case, however, a similar unexplained improvement in affinity is seen with the nucleotide inhibitor 2′-CMP, suggesting that Gln12 may impede ligand binding at P_1 more generally through some mechanism that cannot be discerned from the ANG crystal structure.

Although the experimental findings support the general binding modes observed in the computational models, we do not expect that the models correspond in detail to the actual three-dimensional structures of the ANG−inhibitor complexes. All available docking procedures, including AutoDock, are compromised by theoretical gaps pertaining to thermodynamic and quantum-mechanical aspects of protein−ligand interactions (see refs *63* and *64*). Further, water molecules can make significant contributions to ligand binding and are often included explicitly in docking calculations when their importance to inhibitor interactions is supported by structural data; however, no such information was available for ANG−inhibitor complexes, and we therefore excluded all of the crystallographically observed water molecules. Finally, the docking method used here does not take into account changes in receptor structure associated with ligand binding. This limitation may be particularly relevant to ANG, which undergoes an as yet uncharacterized conformational change involving the C-terminal segment of residues 117−123 (*28*, *43*) to accommodate RNA substrates. In the crystal structure of free ANG, residues 117−120 are well-fixed (temperature factors are low, and several interactions are formed with outside residues), whereas residues 121−123 are flexible and have only weak density. We found that it was only possible to obtain a realistic docking position for compound **1b** when these latter residues were deleted from the ANG structure. A previous study on thymidylate synthase had emphasized the importance of taking into account such "soft spots" for structure-based drug design (*65*). The consistency between the docking and experimental results with our inhibitors suggests that these compounds do not induce a repositioning of the entire segment of residues 117−123. However, this possibility cannot be excluded.

The kinetic and docking results suggest some specific approaches for the rational design of more effective ANG inhibitors. The ionic interactions of these compounds with the P_1 and P_2 subsites of ANG appear to be important and should probably be maintained (or, if possible, strengthened) in the core scaffold of any new analogues. Combinatorial methods may prove to be useful in identifying favorable R groups to attach to these scaffolds, especially on the side that approaches the flexible C-terminal region. For analogues of the compound **2** series (**2**, **2a**, and **2b**), it should be advantageous to avoid the type of symmetry that is characteristic of the parent structures, given the quite dissimilar natures of the sites in which the R groups are expected to bind. Our findings also suggest ways in which inhibitor selectivity might be improved. Compounds **2a** and **2b** appear to utilize the B_2 subsite of ANG, which is much more open than those in the other RNases (*43*, *66*−*68*). The component of these inhibitors that occupies site B_2 cannot be accommodated in the corresponding subsite of pancreatic RNase (or the other enzymes, results not shown), but the flexibility of the compounds allows the conflict to be averted. Modifications that enlarge or rigidify this part of the inhibitor structure might then be highly advantageous. Extension of inhibitors farther into site B_2 might produce an additional benefit: residues in or adjacent to this region are thought to form part of a critical cell-binding site of ANG (*69*), and these compounds might therefore serve as "double-barreled" antagonists that simultaneously inhibit the ribonucleolytic action of ANG and hinder interactions with cellular targets.

ACKNOWLEDGMENT

We thank the National Cancer Institute (NCI) Developmental Therapeutics Program for samples of repository compounds, Drs. Roger Haugwitz and Ven Narayanan of NCI for helpful discussions, the Harvard Institute of Chemistry and Cell Biology for the use of LC−MS equipment, Dr. Nello Russo for providing Q117G and des(121−123), and Cecilia Roh and Marsha Crochiere for excellent technical assistance.

SUPPORTING INFORMATION AVAILABLE

Tables of the structures and K_i values for the complete set of compound **1** and compound **2** analogues that were tested and K_i values for selected inhibitors with ANG variants. This material is available free of charge via the Internet at http://pubs.acs.org.

REFERENCES

1. Kurachi, K., Davie, E. W., Strydom, D. J., Riordan, J. F., and Vallee, B. L. (1985) Sequence of the cDNA and gene for angiogenin, a human angiogenesis factor, *Biochemistry 24*, 5494−5499.
2. Fett, J. W., Strydom, D. J., Lobb, R. R., Alderman, E. M., Bethune, J. L., Riordan, J. F., and Vallee, B. L. (1985) Isolation and characterization of angiogenin, an angiogenic protein from human carcinoma cells, *Biochemistry 24*, 5480−5486.
3. Shapiro, R., Riordan, J. F., and Vallee, B. L. (1986) Characteristic ribonucleolytic activity of human angiogenin, *Biochemistry 25*, 3527−3532.
4. Shapiro, R., Weremowicz, S., Riordan, J. F., and Vallee, B. L. (1987) Ribonucleolytic activity of angiogenin: essential histidine, lysine, and arginine residues, *Proc. Natl. Acad. Sci. U.S.A. 84*, 8783−8787.
5. Harper, J. W., and Vallee, B. L. (1989) A covalent angiogenin/ribonuclease hybrid with a fourth disulfide bond generated by regional mutagenesis, *Biochemistry 28*, 1875−1884.
6. Shapiro, R., Fox, E. A., and Riordan, J. F. (1989) Role of lysines in human angiogenin: chemical modification and site-directed mutagenesis, *Biochemistry 28*, 1726−1732.
7. Shapiro, R., and Vallee, B. L. (1989) Site-directed mutagenesis of histidine-13 and histidine-114 of human angiogenin. Alanine derivatives inhibit angiogenin-induced angiogenesis, *Biochemistry 28*, 7401−7408.
8. Curran, T. P., Shapiro, R., and Riordan, J. F. (1993) Alteration of the enzymatic specificity of human angiogenin by site-directed mutagenesis, *Biochemistry 32*, 2307−2313.

9. Kao, R. Y., Jenkins, J. L., Olson, K. A., Key, M. E., Fett, J. W., and Shapiro, R. (2002) A small-molecule inhibitor of the ribonucleolytic activity of human angiogenin that possesses antitumor activity, *Proc. Natl. Acad. Sci. U.S.A. 99*, 10066−10071.
10. Moroianu, J., and Riordan, J. F. (1994) Nuclear translocation of angiogenin in proliferating endothelial cells is essential to its angiogenic activity, *Proc. Natl. Acad. Sci. U.S.A. 91*, 1677−1681.
11. Xu, Z. P., Tsuji, T., Riordan, J. F., and Hu, G. F. (2002) The nuclear function of angiogenin in endothelial cells is related to rRNA production, *Biochem. Biophys. Res. Commun. 294*, 287−292.
12. Shapiro, R. (1998) Structural features that determine the enzymatic potency and specificity of human angiogenin: threonine-80 and residues 58−70 and 116−123, *Biochemistry 37*, 6847−6856.
13. Etoh, T., Shibuta, K., Barnard, G. F., Kitano, S., and Mori, M. (2000) Angiogenin expression in human colorectal cancer: the role of focal macrophage infiltration, *Clin. Cancer Res. 6*, 3545−3551.
14. Shimoyama, S., Gansauge, F., Gansauge, S., Negri, G., Oohara, T., and Beger, H. G. (1996) Increased angiogenin expression in pancreatic cancer is related to cancer aggressiveness, *Cancer Res. 56*, 2703−2706.
15. Eberle, K., Oberpichler, A., Trantakis, C., Krupp, W., Knupfer, M., Tschesche, H., and Seifert, V. (2000) The expression of angiogenin in tissue samples of different brain tumours and cultured glioma cells, *Anticancer Res. 20*, 1679−1684.
16. Olson, K. A., Byers, H. R., Key, M. E., and Fett, J. W. (2001) Prevention of human prostate tumor metastasis in athymic mice by antisense targeting of human angiogenin, *Clin. Cancer Res. 7*, 3598−3605.
17. Olson, K. A., Byers, H. R., Key, M. E., and Fett, J. W. (2002) Inhibition of prostate carcinoma establishment and metastatic growth in mice by an antiangiogenin monoclonal antibody, *Int. J. Cancer 98*, 923−929.
18. Gho, Y. S., Yoon, W. H., and Chae, C. B. (2002) Antiplasmin activity of a peptide that binds to the receptor-binding site of angiogenin, *J. Biol. Chem. 277*, 9690−9694.
19. Russo, N., Acharya, K. R., Vallee, B. L., and Shapiro, R. (1996) A combined kinetic and modeling study of the catalytic center subsites of human angiogenin, *Proc. Natl. Acad. Sci. U.S.A. 93*, 804−808.
20. Russo, A., Acharya, K. R., and Shapiro, R. (2001) Small molecule inhibitors of RNase A and related enzymes, *Methods Enzymol. 341*, 629−468.
21. Leonidas, D. D., Shapiro, R., Allen, S. C., Subbarao, G. V., Veluraja, K., and Acharya, K. R. (1999) Refined crystal structures of native human angiogenin and two active site variants: implications for the unique functional properties of an enzyme involved in neovascularisation during tumour growth, *J. Mol. Biol. 285*, 1209−1233.
22. Leonidas, D. D., Chavali, G. B., Jardine, A. M., Li, S., Shapiro, R., and Acharya, K. R. (2001) Binding of phosphate and pyrophosphate ions at the active site of human angiogenin as revealed by X-ray crystallography, *Protein Sci. 10*, 1669−1676.
23. Halperin, I., Buyong, M., Wolfson, H., and Nussinov, R. (2002) Principles of docking: an overview of search algorithms and a guide to scoring functions, *Proteins 47*, 409−443.
24. Taylor, R. D., Jewsbury, P. J., and Essex, J. W. (2002) A review of protein-small molecule docking methods, *J. Comput.-Aided Mol. Des. 16*, 151−166.
25. Jenkins, J. L., Kao, R. Y. T., and Shapiro, R. (2003) Virtual screening to enrich hit lists from high-throughput screening: A case study on small-molecule inhibitors of angiogenin, *Proteins 50*, 81−93.
26. Morris, G. M., Goodsell, D. S., Halliday, R. S., Huey, R., Hart, W. E., Belew, R. K., and Olson, A. J. (1998) Automated docking using a Lamarckian genetic algorithm and an empirical binding free energy function, *J. Comput. Chem. 19*, 1639−1662.
27. Shapiro, R., and Vallee, B. L. (1992) Identification of functional arginines in human angiogenin by site-directed mutagenesis, *Biochemistry 31*, 12477−12485.
28. Russo, N., Shapiro, R., Acharya, K. R., Riordan, J. F., and Vallee, B. L. (1994) Role of glutamine-117 in the ribonucleolytic activity of human angiogenin, *Proc. Natl. Acad. Sci. U.S.A. 91*, 2920−2924.
29. Russo, N., Nobile, V., Di Donato, A., Riordan, J. F., and Vallee, B. L. (1996) The C-terminal region of human angiogenin has a dual role in enzymatic activity, *Proc. Natl. Acad. Sci. U.S.A. 93*, 3243−3247.
30. Chen, C. Z., and Shapiro, R. (1997) Site-specific mutagenesis reveals differences in the structural bases for tight binding of RNase inhibitor to angiogenin and RNase A, *Proc. Natl. Acad. Sci. U.S.A. 94*, 1761−1766.
31. Shapiro, R., Harper, J. W., Fox, E. A., Jansen, H. W., Hein, F., and Uhlmann, E. (1988) Expression of Met-(−1) angiogenin in *Escherichia coli*: conversion to the authentic <Glu-1 protein, *Anal. Biochem. 175*, 450−461.
32. Russo, N., and Shapiro, R. (1999) Potent inhibition of mammalian ribonucleases by 3′,5′-pyrophosphate-linked nucleotides, *J. Biol. Chem. 274*, 14902−14908.
33. Green, F. J. (1990) *The Sigma-Aldrich handbook of stains, dyes, and indicators*, Aldrich Chemical Co., Milwaukee.
34. Ewing, T. J., Makino, S., Skillman, A. G., and Kuntz, I. D. (2001) DOCK 4.0: search strategies for automated molecular docking of flexible molecule databases, *J. Comput.-Aided Mol. Des. 15*, 411−428.
35. Hart, T. N., Ness, S. R., and Read, R. J. (1997) Critical evaluation of the research docking program for the CASP2 challenge, *Proteins* (Suppl. 1), 205−209.
36. Bohm, H. J. (1994) The development of a simple empirical scoring function to estimate the binding constant for a protein−ligand complex of known three-dimensional structure, *J. Comput.-Aided Mol. Des. 8*, 243−256.
37. Leland, P. A., Staniszewski, K. E., Park, C., Kelemen, B. R., and Raines, R. T. (2002) The ribonucleolytic activity of angiogenin, *Biochemistry 41*, 1343−1350.
38. Shapiro, R., Fett, J. W., Strydom, D. J., and Vallee, B. L. (1986) Isolation and characterization of a human colon carcinoma-secreted enzyme with pancreatic ribonuclease-like activity, *Biochemistry 25*, 7255−7264.
39. Morrison, J. F. (1969) Kinetics of the reversible inhibition of enzyme-catalysed reactions by tight-binding inhibitors, *Biochim. Biophys. Acta 185*, 269−286.
40. Jardine, A. M., Leonidas, D. D., Jenkins, J. L., Park, C., Raines, R. T., Acharya, K. R., and Shapiro, R. (2001) Cleavage of 3′,5′-pyrophosphate-linked dinucleotides by ribonuclease A and angiogenin, *Biochemistry 40*, 10262−10272.
41. Richards, F. M., and Wyckoff, H. W. (1971) Bovine pancreatic ribonuclease, *Enzymes (3rd Ed.) 4*, 647−806.
42. Raines, R. T. (1998) Ribonuclease A, *Chem. Rev. 98*, 1045−1065.
43. Acharya, K. R., Shapiro, R., Allen, S. C., Riordan, J. F., and Vallee, B. L. (1994) Crystal structure of human angiogenin reveals the structural basis for its functional divergence from ribonuclease, *Proc. Natl. Acad. Sci. U.S.A. 91*, 2915−2919.
44. Leonidas, D. D., Shapiro, R., Subbarao, G. V., Russo, A., and Acharya, K. R. (2002) Crystallographic studies on the role of the C-terminal segment of human angiogenin in defining enzymatic potency, *Biochemistry 41*, 2552−2562.
45. Fontecilla-Camps, J. C., de Llorens, R., le Du, M. H., and Cuchillo, C. M. (1994) Crystal structure of ribonuclease A•d(ApTpApApG) complex. Direct evidence for extended substrate recognition, *J. Biol. Chem. 269*, 21526−21531.
46. Boix, E., Nogues, M. V., Schein, C. H., Benner, S. A., and Cuchillo, C. M. (1994) Reverse transphosphorylation by ribonuclease A needs an intact p2-binding site. Point mutations at Lys-7 and Arg-10 alter the catalytic properties of the enzyme, *J. Biol. Chem. 269*, 2529−2534.
47. Zacharias, N., and Dougherty, D. A. (2002) Cation-pi interactions in ligand recognition and catalysis, *Trends Pharmacol. Sci. 23*, 281−287.
48. Harper, J. W., and Vallee, B. L. (1988) Mutagenesis of aspartic acid-116 enhances the ribonucleolytic activity and angiogenic potency of angiogenin, *Proc. Natl. Acad. Sci. U.S.A. 85*, 7139−7143.
49. Fisher, B. M., Schultz, L. W., and Raines, R. T. (1998) Coulombic effects of remote subsites on the active site of ribonuclease A, *Biochemistry 37*, 17386−17401.
50. Lequin, O., Thuring, H., Robin, M., and Lallemand, J. Y. (1997) Three-dimensional solution structure of human angiogenin determined by ^{1}H,^{15}N NMR spectroscopy: characterization of histidine protonation states and pK_a values, *Eur. J. Biochem. 250*, 712−726.

51. delCardayre, S. B., Ribo, M., Yokel, E. M., Quirk, D. J., Rutter, W. J., and Raines, R. T. (1995) Engineering ribonuclease A: production, purification and characterization of wild-type enzyme and mutants at Gln11, *Protein Eng. 8*, 261−273.
52. Irie, M. (1965) Effects of salts on the reaction of bovine pancreatic RNase A, *J. Biochem. 57*, 355−362.
53. Park, C., and Raines, R. T. (2001) Quantitative analysis of the effect of salt concentration on enzymatic catalysis, *J. Am. Chem. Soc. 123*, 11472−11479.
54. Beintema, J. J., and Kleineidam, R. G. (1998) The ribonuclease A superfamily: general discussion, *Cell. Mol. Life Sci. 54*, 825−832.
55. Zhang, J., Dyer, K. D., and Rosenberg, H. F. (2002) RNase 8, a novel RNase A superfamily ribonuclease expressed uniquely in placenta, *Nucleic Acids Res. 30*, 1169−1175.
56. Pous, J., Canals, A., Terzyan, S. S., Guasch, A., Benito, A., Ribo, M., Vilanova, M., and Coll, M. (2000) Three-dimensional structure of a human pancreatic ribonuclease variant, a step forward in the design of cytotoxic ribonucleases, *J. Mol. Biol. 303*, 49−60.
57. Landre, J. B., Hewett, P. W., Olivot, J. M., Friedl, P., Ko, Y., Sachinidis, A., and Moenner, M. (2002) Human endothelial cells selectively express large amounts of pancreatic-type ribonuclease (RNase 1), *J. Cell. Biochem. 86*, 540−552.
58. Rosenberg, H. F. (1998) The eosinophil ribonucleases, *Cell. Mol. Life Sci. 54*, 795−803.
59. Hofsteenge, J., Vicentini, A., and Zelenko, O. (1998) Ribonuclease 4, an evolutionarily highly conserved member of the superfamily, *Cell. Mol. Life Sci. 54*, 804−810.
60. Kumar, K., Jenkins, J. L., Jardine, A. M., and Shapiro, R. (2003) Inhibition of mammalian ribonucleases by endogenous adenosine dinucleotides, *Biochem. Biophys. Res. Commun. 300*, 81−86.
61. Shapiro, R., Strydom, D. J., Olson, K. A., and Vallee, B. L. (1987) Isolation of angiogenin from normal human plasma, *Biochemistry 26*, 5141−5146.
62. Blaser, J., Triebel, S., Kopp, C., and Tschesche, H. (1993) A highly sensitive immunoenzymometric assay for the determination of angiogenin, *Eur. J. Clin. Chem. Clin. Biochem. 31*, 513−516.
63. Mestres, J., and Knegtel, R. M. A. (2000) Similarity versus docking in 3D virtual screening, *Perspect. Drug Discovery Des. 20*, 191−207.
64. Ajay, and Murcko, M. A. (1995) Computational methods to predict binding free energy in ligand−receptor complexes, *J. Med. Chem. 38*, 4953−4967.
65. Fritz, T. A., Tondi, D., Finer-Moore, J. S., Costi, M. P., and Stroud, R. M. (2001) Predicting and harnessing protein flexibility in the design of species-specific inhibitors of thymidylate synthase, *Chem. Biol. 8*, 981−995.
66. Wlodawer, A., Svensson, L. A., Sjolin, L., and Gilliland, G. L. (1988) Structure of phosphate-free ribonuclease A refined at 1.26 Å, *Biochemistry 27*, 2705−2717.
67. Terzyan, S. S., Peracaula, R., de Llorens, R., Tsushima, Y., Yamada, H., Seno, M., Gomis-Ruth, F. X., and Coll, M. (1999) The three-dimensional structure of human RNase 4, unliganded and complexed with d(Up), reveals the basis for its uridine selectivity, *J. Mol. Biol. 285*, 205−214.
68. Boix, E., Leonidas, D. D., Nikolovski, Z., Nogues, M. V., Cuchillo, C. M., and Acharya, K. R. (1999) Crystal structure of eosinophil cationic protein at 2.4 Å resolution, *Biochemistry 38*, 16794−16801.
69. Hallahan, T. W., Shapiro, R., and Vallee, B. L. (1991) Dual site model for the organogenic activity of angiogenin, *Proc. Natl. Acad. Sci. U.S.A. 88*, 2222−2226.

BI034164E